

# Geophysical Research Letters®

## RESEARCH LETTER

10.1029/2021GL094698

### Key Points:

- We classify long-period, volcano-tectonic, and hybrid events by spectral dissimilarity and hierarchical clustering
- The unusual high seismicity rate and more shallow origins in the last episode in April 9–27 may be indicative of the impending eruption
- The spatiotemporal patterns of hybrid events shed light on their physical mechanisms

### Supporting Information:

Supporting Information may be found in the online version of this article.

### Correspondence to:

Z. Li,  
[zefengli@ustc.edu.cn](mailto:zefengli@ustc.edu.cn)

### Citation:

Cui, X., Li, Z., & Huang, H. (2021). Subdivision of seismicity beneath the summit region of Kilauea volcano: Implications for the preparation process of the 2018 eruption. *Geophysical Research Letters*, 48, e2021GL094698. <https://doi.org/10.1029/2021GL094698>

Received 11 JUN 2021

Accepted 10 OCT 2021

## Subdivision of Seismicity Beneath the Summit Region of Kilauea Volcano: Implications for the Preparation Process of the 2018 Eruption

Xin Cui<sup>1</sup> , Zefeng Li<sup>1,2</sup> , and Hui Huang<sup>3</sup>

<sup>1</sup>Laboratory of Seismology and Physics of Earth's Interior, School of Earth and Space Sciences, University of Science and Technology of China, Hefei, China, <sup>2</sup>Mengcheng National Geophysical Observatory, University of Science and Technology of China, Mengcheng, China, <sup>3</sup>Department of Earth Sciences, University of Oxford, Oxford, UK

**Abstract** Long-period (LP), hybrid, and volcano-tectonic (VT) seismicity are important indicators for tracking the evolution of volcanic processes. Here, we propose an unsupervised learning method to classify 5,949 seismic events in Kilauea volcano, Hawai'i, during a 4-month period before the collapse of Pu'u' O'o on April 30, 2018. The LPs and hybrids exhibit three major episodes, which progressively intensified and had increasing shallow events toward the eruption. The most intense episode starting 3 weeks before eruption coincides with changes in near-caldera deformation and lava lake elevation in Halema'uma'u, serving as possible immediate precursors. However, the first two episodes imply magma migration was already active months prior to the eruption. The spatiotemporal patterns of abundant hybrids reveal that they are associated with magma movement but mixed with shear-failure or near-surface resonance. Our results provide useful constraints on the magmatic processes in the preparation phase of the Kilauea eruption in 2018.

**Plain Language Summary** Many volcanoes around the world have been known to produce different types of seismic events, which can be used to infer volcanic processes underneath. However, classification of these events remains a challenging task. We propose a new classification method and apply it to numerous seismic events in Kilauea volcano, Hawai'i, before the collapse of Pu'u' O'o in 2018. We successfully separate different types of events and observe interesting spatiotemporal patterns. The results show that, before the eruption, the long-period and hybrid events have three episodes. Together with surface observations, the latest episode in April 9–27 shows an unusually high rate and more shallow origins, indicative of the impending eruption. In addition, the spatiotemporal patterns of hybrid events shed light on their physical mechanisms. These results provide useful constraints on the magma migration processes in the preparation phase of the Kilauea eruption in 2018.

## 1. Introduction

Seismicity is one of the most important indicators in volcano monitoring and eruption forecasting. Volcanic processes involving multiphase materials and geometrically complex structures result in diverse types of seismic events (Chouet, 1996; McNutt, 1996; Sparks, 2003; Woods et al., 2018). Long-period (LP) events, with dominant frequencies from 0.5 to 5 Hz, are thought to be generated by fluid-filled resonators (Aki et al., 1977; Chouet, 1988; Chouet & Matoza, 2013; Neuberg et al., 2000), and closely related to magma transport and shallow hydrothermal activity (Chouet, 1996; Jousset et al., 2013). LP swarms are often observed preceding volcano eruptions (Chouet, 1996), although their occurrence does not always lead to eruptions (Matoza et al., 2014; Okubo & Nakata, 2003). Volcano-tectonic (VT) events have a peak frequency between 5 and 15 Hz. They are typically considered as brittle rock failure within a volcanic edifice triggered by stress changes (Chouet & Matoza, 2013; McNutt & Roman, 2015), and in turn are useful to infer the edifice's stress state (Duputel et al., 2019).

A special class of volcanic seismicity called hybrids contains mixed frequency contents of LPs and VTs. However, hybrids are often much less populated than LPs and VTs. Moreover, the exact causes of hybrids are obscure, partly due to a limited number of available observations (Chouet & Matoza, 2013; McNutt & Roman, 2015). Previous studies have proposed several possible mechanisms: (a) hybrids are LPs triggered by shear-failure (Chouet & Matoza, 2013; Foulger et al., 2004); (b) hybrids are LPs with unattenuated high

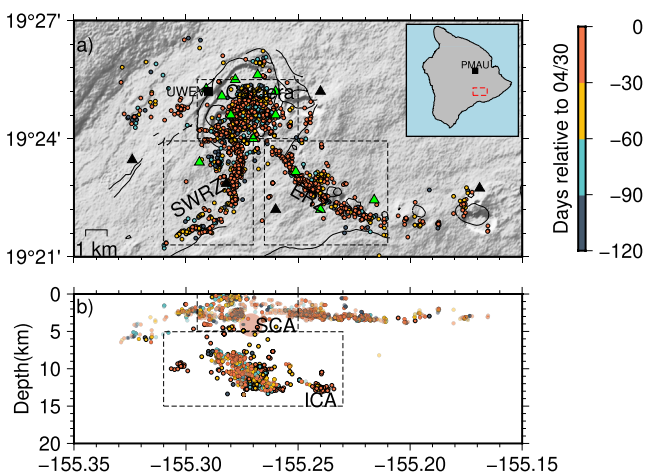


**Figure 1.** The seismicity in Kilauea summit region from January 1, 2018 to April 30, 2018. (a) Seismicity is color coded by their occurrence time relative to April 30, 2018. Black lines delineate major faults and the Halema'uma'u caldera. Triangles denote 5 short-period (black) and 12 broadband stations (green) used in this study. UWEV (155.29 W, 19.42 N) and PMAU (155.32 W, 19.76 N; black squares) are continuous GPS stations. The study area is divided into three subregions for convenience of discussion: Caldera (CA), Southwest Rift Zone (SWRZ), and East Rift Zone (ERZ). (b) Depth profile of seismicity. Depth is relative to sea level. The light red shading represents the shallow magma reservoir. The seismicity beneath the caldera is divided into shallow (0–5 km, SCA), and intermediate deep (5–15 km, ICA) depth.

2018. The 4-month seismicity forms five general groups, which belong to LPs, hybrids, and VTs, respectively. Distinct spectral characteristics and spatiotemporal patterns of these events are observed. Moreover, the large number of hybrids provides tight constraints on their underlying mechanisms in Kilauea.

## 2. Data and Methods

On April 30, 2018, a dike intruded downrift from Pu'u' O'o into the lower east rift zone (LERZ), kicking off a series of eruptions and collapse events in Kilauea volcano (Neal et al., 2019). A large number of seismic events around the Kilauea summit area were recorded by the USGS Hawaiian Volcano Observatory (HVO) seismic network. Huang & Meng, 2018 applied a template-matching technique to recover numerous small events missing in standard HVO catalogs and relocated them with a double-difference method (Waldhauser & Ellsworth, 2000). The enhanced catalog provides a unique opportunity to investigate the detailed evolution of seismicity in response to the magmatic processes during the preparation phase.

We focus on the events from January 1 to April 30, 2018 (Figure 1). The event waveforms are cut on the vertical component of 17 HVO broadband and short-period stations near the summit region (Figure 1). They are preprocessed with mean removal, instrumental correction, and fourth-order 1–15 Hz Butterworth band-pass filtering. The P-wave arrivals are picked by recursive STA/LTA (Withers et al., 1998). We calculate the signal-to-noise ratio (SNR) on each station and only keep 5,949 high-quality events which are recorded by more than five stations with  $\text{SNR} > 3$  dB. For each event, we compute the P wave spectra for the recording stations with a 2.56-s window, 1.28 s before and after the arrival (Matoza et al., 2014; Shearer et al., 2006). The spectra are normalized to unit area in order to retain the relative energy distribution information. Because the frequency content varies with stations, for each event, we select the representative spectrum that has median FI among the recording stations (Matoza et al., 2014).

The dissimilarity between two events is defined as the Euclidean distance of their respective spectra:

frequency content (Neuberg et al., 2006); (c) hybrids are shear failure with slow rupture and complex path effects (Harrington & Brodsky, 2007). A detailed spatiotemporal pattern of an abundance of hybrids would be important to clarify their exact causes.

To help illuminate the magmatic processes prior to eruption and shed light on the mechanisms of hybrids, high-quality catalogs of LPs, VTs, and hybrids are essential. Unfortunately, reliable automatic classification of a large number of events is a challenging task. Frequency index (FI), proposed by Buurman and West (2010), is widely used (Ketner & Power, 2013; Matoza et al., 2014; Wech & Thelen, 2015; Woods et al., 2018). It is defined as

$$\text{FI} = \log_{10} \frac{\bar{A}_{\text{upper}}}{\bar{A}_{\text{lower}}} \quad (1)$$

where  $\bar{A}_{\text{upper}}$  and  $\bar{A}_{\text{lower}}$  are the average spectral amplitudes within high frequency and low frequency bands, respectively. The FI values of volcanic seismicity tend to overlap in the intermediate range, resulting in ambiguity in classifying the hybrids and part of the LPs and VTs (Matoza et al., 2014).

Here, to illuminate the magmatic processes in the preparation phase of the Kilauea eruption in 2018, we propose a two-step method to classify volcanic seismicity without ambiguity. Our method consists of hierarchical clustering based on pair-wise comparison of P wave spectra, followed by regrouping in a 2-D feature space of dominant frequency and spectral width. We take advantage of a high-quality earthquake catalog (Huang & Meng, 2018) around the summit region within 4 months before April 30,

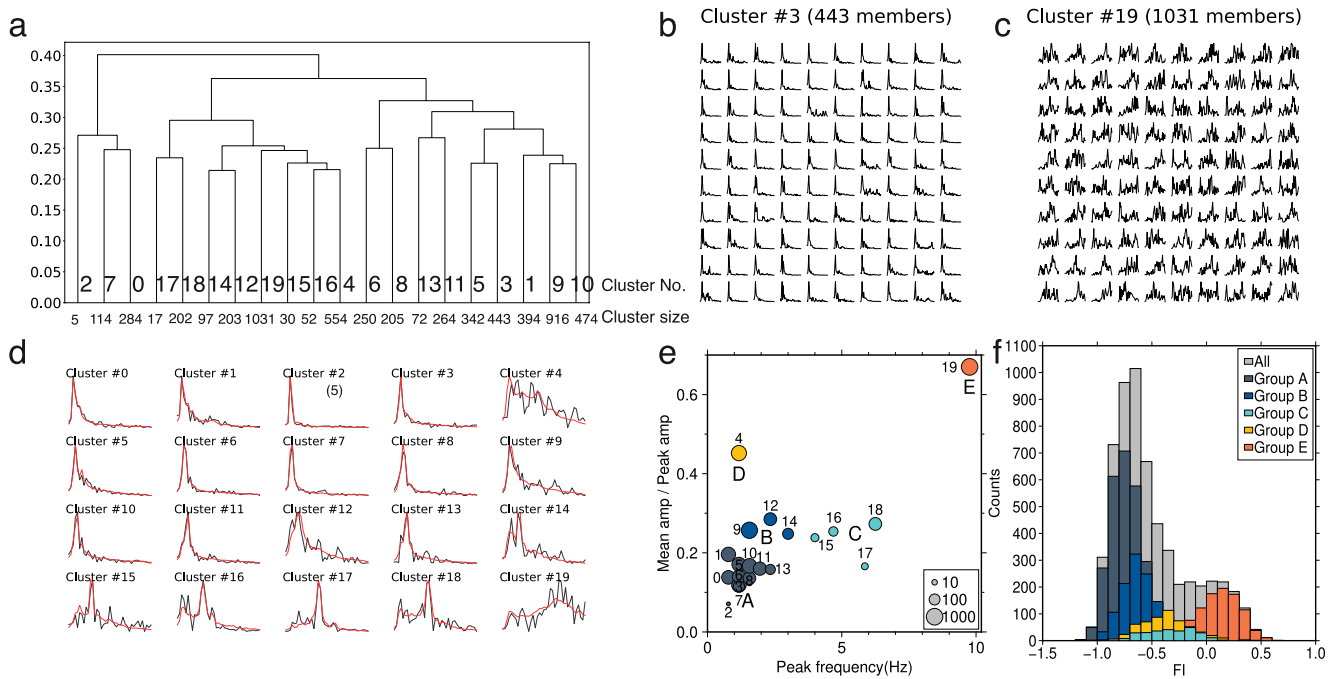


**Figure 2.** Hierarchical clustering and regrouping of seismicity in Kilauea. (a) Dendrogram of seismicity divided into 20 clusters based on the dissimilarity of P-wave spectra. (b) Examples of long-period spectra for Cluster 3 (443 members in total, 100 randomly selected are shown). (c) Examples of high-frequency spectra for Cluster 19 (1,031 members in total, 100 randomly selected are shown). (d) Average spectra (red) and median spectra (black) of 20 clusters. (e) Regrouping the 20 clusters in a feature space: peak frequency versus spectral mean/maximum ratio measured from their average spectra. Clusters are grouped based on their proximity in the feature space. The size is proportional to the logarithm of cluster size. (f) Frequency-index distribution of all (gray) and the five groups (colored).

$$d(A_1, A_2) = \sqrt{\sum_{f=0}^{15\text{ Hz}} \|A_1(f) - A_2(f)\|^2} \quad (2)$$

where  $A_1(f)$  and  $A_2(f)$  are amplitudes at frequency  $f$  for event 1 and 2, respectively. This metric is computed for all possible event pairs, which forms a dissimilarity matrix (Figure S1 in Supporting Information S1). With the dissimilarity matrix, hierarchical clustering begins with each event as an individual cluster, and then gradually merges them from high to low similarity. This process is repeated until a preset number of clusters are formed (Figure 2a). Here we arbitrarily set 20 clusters, which tends to overly divide the events at this step (i.e., some similar events may be divided into finer clusters). Figures 2b and 2c show a low-frequency cluster (Cluster 3) and a high-frequency cluster (Cluster 19), respectively. Figure S2 in Supporting Information S1 shows the other 18 clusters and Figure S3 in Supporting Information S1 shows the example waveforms for all the clusters.

The average spectra of 20 clusters (Figure 2d) suggest that many clusters (e.g., Clusters 0, 1, 3, 6) share similar spectra and therefore further merging is needed. The average spectra show that peak frequency and frequency bandwidth are key features to distinguish different clusters. We quantify the bandwidth by a ratio of mean to maximum spectral amplitude: near zero suggests concentrated energy at a given frequency (harmonic), whereas near one suggests a flat spectrum (broadband). In the feature space, the clusters are merged to five general groups (Figure 2e). Group A consists of Clusters 0, 1, 2, 3, 5, 6, 7, 8, 10, 11, 13, which have harmonic frequency and peak frequency at 0.5–3 Hz. Group B consists of Cluster 9, 12, 14, which have slightly wider spectra. Group C consists of Clusters 15, 16, 17, 18, which have peak frequency between 4 and 6 Hz. It is somewhat arbitrary to assign Cluster 15 to Group C or Group B; however, the result remains largely the same because it only has 30 members. Cluster 4 alone forms Group D, which has double spectral peaks and broadband frequency contents. Cluster 19 alone forms Group E, which has the highest dominant frequency and is the most broadband.

It is noteworthy that the pre-clustering based on spectral Euclidean distance is important to reduce the impact of noise on evaluating the overall similarity of spectra. In fact, the distribution of all events in the feature space is generally consistent with previous grouping (Figure S5 in Supporting Information S1). However, because the peak frequency is vulnerable to noise contamination, direct clustering of all events in the feature space may not yield reliable results. For example, a broadband event that happens to have an insignificant peak at long periods (Figure S5 in Supporting Information S1) could be falsely classified to the long-period group B or the hybrid group D because the proximity in the feature space. However, the two-step method correctly categorizes it as a broadband event using the whole spectral shape.

### 3. Results

We compare our grouping with the FI distribution. The station-averaged FIs of all the events in the 4 months show a bimodal distribution (Figure 2f), in agreement of long-term historic events in Kilauea (Matoza et al., 2014). The grouping, however, reveals the detailed composition of the bimodal distribution (Figure 2f). Groups A and B dominate the lowest and second lowest FIs, corresponding to the range of LPs (Buurman & West, 2010; Chouet & Matoza, 2013; Matoza et al., 2014). Groups C and D are composed of the intermediate FIs, corresponding to the range of hybrids (Lahr et al., 1994; Neuberg et al., 2000; Neuberg et al., 2006). Group E dominates the highest FIs, corresponding to the range of VTs (Chouet & Matoza, 2013). Hence, the ambiguity of classifying the LPs, VTs, and hybrids in the overlapping FI range is cleared.

To illustrate the spatial patterns, the study area is divided into shallow (SCA, 0–5 km), intermediate deep (ICA, 5–15 km) caldera, southwest rift zone (SWRZ), and east rift zone (ERZ) (Figure 1). Groups A–D are mostly in ICA (Figures 3a–3c, and 3d), whereas Group E was mainly in shallow rift zones. Group C appears to have different preferential spots in the ICA from Groups A and B (Figure S4 in Supporting Information S1). Also, a portion of Group D is found in SCA, SWRZ, and ERZ (Figure 3d). Temporally, Groups A–D had three main episodes before eruption, that is, January 23–February 11, March 1–14, and April 9–27 (Figure 3), whereas Group E steadily increased over the 4-month period and accelerated about 3 weeks before the eruption (Figure 3e).

Taking the FI distribution and spatiotemporal patterns together, Groups A and B have harmonic low-frequency, episodic behaviors and originate from the intermediate depth caldera, demonstrating that they are associated with magma transport, consistent with previous observations of LPs (Battaglia, 2003; Matoza et al., 2014; Wolfe et al., 2004). The VT Group E has high frequency and broadband features, and is mostly located in the shallow region, thus representing brittle-failure sources (Chouet & Matoza, 2013). Groups C and D both have pronounced double peak frequencies, suggesting mixed motion at the waveform onset, consistent with the definition of hybrids (Lahr et al., 1994). However, the spectral and spatial differences imply that the two subtypes of hybrids might have different mechanisms.

## 4. Discussion and Conclusions

### 4.1. Magma Migration in Preparation Phase

The shallow magma reservoir in Kilauea is 3–6 km deep, just above the LPs found in the ICA (Figure 1b; Matoza et al., 2014; Klein et al., 1987). It is noteworthy that the summit magma storage reservoir is generally aseismic. Hence, the LPs reflect the disturbance of unsteady magma flow through the path to the reservoir (Battaglia, 2003; Chouet, 1996; Matoza et al., 2014). The three swarms of LPs and hybrids could signal the episodes of magma infiltration to the reservoir. The three episodes display a progressive intensification in total seismicity and an increasing proportion of shallow events toward the eruption (Figure 4 and Figure S6 in Supporting Information S1). This indicates that the plumbing system was filled with magma influxes batch-by-batch which led up to the eventual collapse of Pu'u' O'o on April 30, 2018.

Specifically, in the first two episodes, the seismicity rate was generally lower (61 and 66 events per day, respectively) and a smaller proportion of LPs (3.1% and 4.2%) occurred in the shallow depth. At these stages, the magma recharged the reservoir but did not make it up near the surface, as evidenced by no significant surface changes of lava lake elevation in the Halema'uma'u crater and GPS deformation data (Figure 3f). In contrast, the last episode was much more active (136 events per day) and more LPs (6.6%) occurred in the

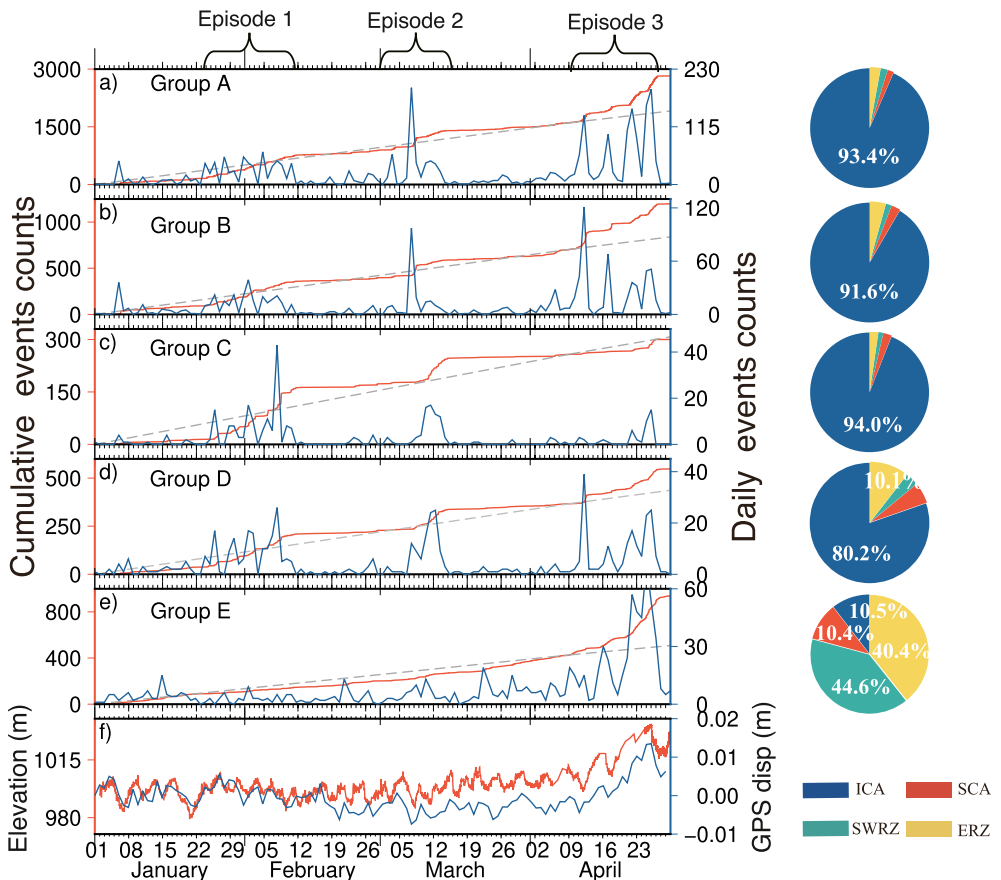


**Figure 3.** Temporal and spatial distribution of the five seismicity groups. (a–e) The left panel: the blue curves show daily event counts (the right Y label). The red curves are cumulative events (the left Y label). The dotted lines show the linear fit of cumulative events from January 1 to April 10, 2018 to highlight the acceleration phase between April 10 and April 30. The right panel: spatial distributions of five seismicity groups. (f) Elevation of the summit lava lake (red curve) after Patrick et al. (2020) and the GPS northward displacement near the summit (blue curve) on station UWEV (Figure 1) after Blewitt et al. (2018).

shallow region. Meanwhile, there was a significant increase in the lava lake elevation and inflation signal in the GPS data. These suggest the magma had likely migrated into the shallow caldera and ERZ in the third episode. It is noteworthy that numerous LPs occurred in the ERZ while few occurred in the SWRZ in the third episode (Figure S6a in Supporting Information S1). Such a difference coincides with the active volcanism in the ERZ and the relative quiescence in the SWRZ in the later eruption phase.

In contrast to the LPs, the VTs serve as an effective proxy for the pressurization state of the near-surface fractures. They show a steady increase over the 4 months instead of episodic behaviors. The distinct temporal characteristics of VTs and LPs suggest that the near-surface response is not fully synchronized to the underneath mass transport. It could be due to stress diffusion over time when the disturbance transfers through the porous and viscoelastic edifice. However, during the third LP episode, the VTs surged simultaneously, indicating that the magma was directly pressurizing the near-surface structures then.

Compared with only surface observations of lava lake and GPS signals, the seismicity is indispensable to illuminate the underneath processes and probe the near-surface stress state. Particularly, the first two episodes suggest the magmatism was already active months before the eruption, which could not be directly observed from surface GPS or lava lake measurements. Similarly, without the shallow LPs, it was difficult to infer whether the magma had intruded into the ERZ in the last episode. These results demonstrate high-quality catalogs of LPs and VTs could play a unique role in volcano forecasting.

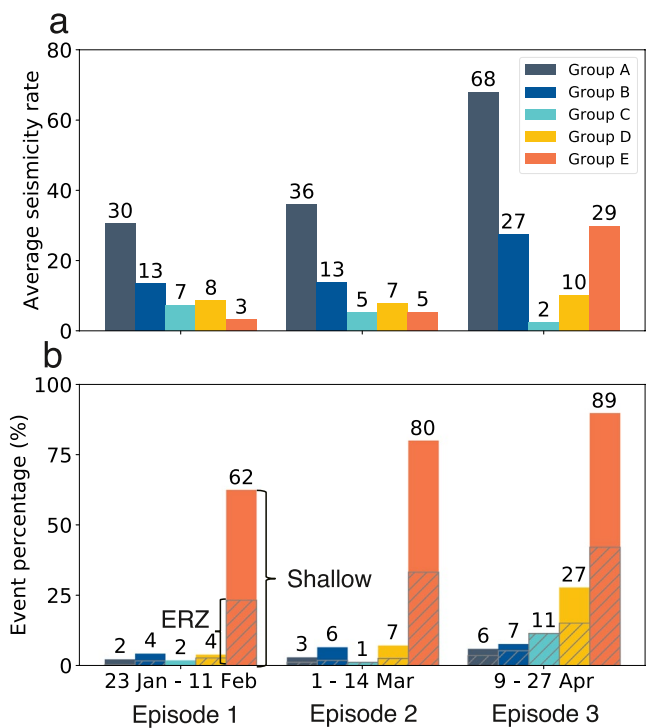


**Figure 4.** The average daily seismicity rate and the proportion of shallow events during three episodes. (a) The average number of events per day within episodes. (b) The proportion of events in the shallow regions (total in SCA, ERZ, and SWRZ) and ERZ within each group.

resonators (e.g., cracks, pipes at  $\sim 100$  m or less). This seems to be supported by >90% events in ICA, similar to Groups A and B (Figure 5). However, more observations are needed to test this hypothesis.

#### 4.3. Potentials and Limitations

Compared to FI—a single feature of the spectrum—our method makes use of the full spectral shape and thus removes the classification ambiguity. Especially, it can separate hybrids which are much less populated and share many similar features with LPs (Figure 5). Moreover, it has minimal assumptions on the event features and can be potentially applied to other volcanos to construct respective catalogs of diverse seismic phenomena and discoveries of new subtypes. Finally, the extracted characteristic spectra (Figure 2d) can serve as a basis for supervised classification that can be implemented in real time. A potential solution is matching the spectra of newly detected events with the characteristic spectra. This remains a subject of future work.

The detailed spatiotemporal patterns of LPs, VTs, and hybrids revealed in this study rely on a high-quality catalog from template-matching and relative location. We compare the standard HVO catalog, which has only 301 events in the same region and time period. Figure S8 in Supporting Information S1 shows that the HVO events generally correlate with three episodes of LPs and steady acceleration of VTs from our study. However, the spatiotemporal patterns are much less significant owing to numerous small events missing in the HVO catalog. This demonstrates a high-quality catalog is important to obtain high-resolution patterns. With adoption of machine learning (Ross et al., 2018; Zhu & Beroza, 2018) and similarity search methods (Senobari et al., 2019; Yoon et al., 2015) in volcano monitoring, we anticipate high-quality catalogs of diverse seismicity to improve our understanding of volcanic processes.

#### 4.2. The Mechanisms of Hybrids

The spatiotemporal patterns of a large set of hybrids in Kilauea provide tight constraints on their controversial causes. Harrington and Brodsky (2007) proposed that the hybrids in Mount St. Helens are brittle-failure with slow rupture velocity and complex propagation effects. However, in Kilauea, the spatial and temporal patterns of both subtypes of hybrids are nearly synchronized with LPs. Therefore, the same driven force, that is, magma movement, must be involved in the generation of hybrids. We also reject another hypothesis that hybrids are LP events with unattenuated high frequency content (e.g., Neuberg et al., 2006). Figure S7 in Supporting Information S1 shows that, at different depths, hybrids and LPs with similar locations all have distinct spectra, which cannot be well explained by attenuation.

We propose that hybrids in Kilauea should be closely associated with LPs and magma movement, but generated in some special settings. Because Group D has a broadband component and a long-period peak (Figure 5), it could be interpreted as a mixture of shear-failure and fluid resonance (Chouet & Matoza, 2013; Foulger et al., 2004). This can explain part of Group D in the rift zones as magma intruded there. Comparatively, Group C has a persistent peak around 5 Hz but the low-frequency component varies widely (Figure S2 in Supporting Information S1, Clusters 15–18). In addition, Figure S7 in Supporting Information S1 shows some depth dependency of the low-frequency component. In fact, the characteristics of Group C agree with the simulation results by Chouet (1996): a 100-m-wide, 200-m-long vertical crack can produce a source-related persistent peak at 3.8 Hz and extra depth-dependent low frequency due to near-surface resonance. If true, Group C is not real hybrids—they are LPs with a higher dominant frequency resulting from small-size fluid-filled

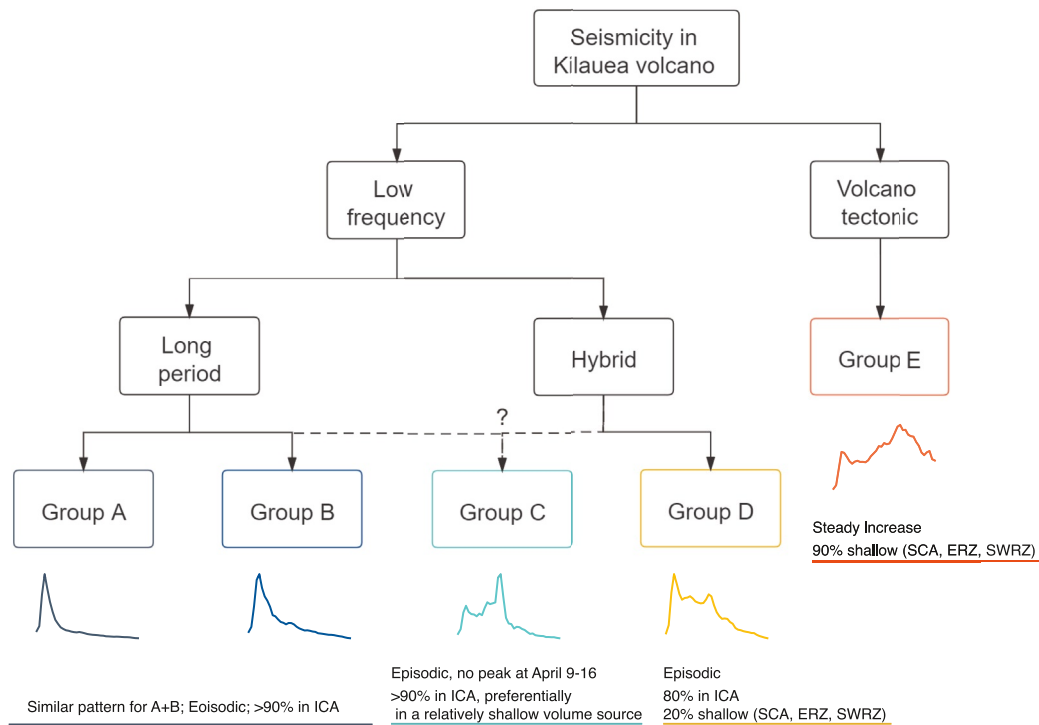


**Figure 5.** Family tree of seismicity types in Kilauea Volcano. Groups A and B represent LPs, mostly in deep caldera and episodic. Group C has a persistent peak around 5 Hz but the low-frequency component varies widely, whose mechanism is still uncleared. Group D has a broadband component and a long period peak, which belongs to hybrids. Both hybrids and LPs are considered to belong to low frequency events. Group E represents VTs, mostly shallow and broadband, showing a steady increase before eruption.

## Data Availability Statement

The seismic data used in this study can be accessed at IRIS (<http://ds.iris.edu/mda/HV/>). The summit lava lake elevation data shared by M.R Patrick is available on ScienceBase (<https://www.sciencebase.gov/catalog/item/5d842627e4b0c4f70d071a23>). The GPS data are downloaded from the Nevada Geodetic Laboratory ([http://geodesy.unr.edu/gps\\_timeseries/tenv3/IGS14/UWEV.tenv3](http://geodesy.unr.edu/gps_timeseries/tenv3/IGS14/UWEV.tenv3)). The cluster analysis code and the template matching catalog used in this study are available at <https://doi.org/10.5281/zenodo.4925485>.

## Acknowledgments

The authors are grateful for Jamie Farrell, two other anonymous reviewers, and the editor Chris Huber for their constructive comments that significantly improved this manuscript. This study is supported by USTC research startup fund to Zefeng Li (Grant No. KY2080000079) and special fund from Institute of Geophysics, China Earthquake Administration (Grant No. DQJB21Z05).

## References

- Aki, K., Fehler, M., & Das, S. (1977). Source mechanism of volcanic tremor: Fluid-driven crack models and their application to the 1963 Kilauea eruption. *Journal of Volcanology and Geothermal Research*, 2(3), 259–287. [https://doi.org/10.1016/0377-0273\(77\)90003-8](https://doi.org/10.1016/0377-0273(77)90003-8)
- Battaglia, J. (2003). Location of long-period events below Kilauea Volcano using seismic amplitudes and accurate relative relocation. *Journal of Geophysical Research*, 108(B12), 2553. <https://doi.org/10.1029/2003JB002517>
- Blewitt, G., Hammond, W., & Kreemer, C. (2018). Harnessing the GPS Data Explosion for Interdisciplinary Science. *Eos*, 99, 485. <https://doi.org/10.1029/2018EO104623>
- Buurman, H., & West, M. E. (2010). *Seismic precursors to volcanic explosions during the 2006 eruption of Augustine Volcano: Chapter 2 in the 2006 eruption of Augustine Volcano, Alaska (USGS Numbered Series No. 1769–2)* (p. 4157). U.S. Geological Survey. Retrieved from <http://pubs.er.usgs.gov/publication/ppl17692>
- Chouet, B. (1988). Resonance of a fluid-driven crack: Radiation properties and implications for the source of long-period events and harmonic tremor. *Journal of Geophysical Research*, 93(B5), 4375–4400. <https://doi.org/10.1029/JB093iB05p04375>
- Chouet, B. A. (1996). Long-period volcano seismicity: Its source and use in eruption forecasting. *Nature*, 380(6572), 309–316. <https://doi.org/10.1038/380309a0>
- Chouet, B. A., & Matzoza, R. S. (2013). A multi-decadal view of seismic methods for detecting precursors of magma movement and eruption. *Journal of Volcanology and Geothermal Research*, 252, 108–175. <https://doi.org/10.1016/j.jvolgeores.2012.11.013>
- Duputel, Z., Lenglé, O., & Ferrazzini, V. (2019). Constraining spatiotemporal characteristics of magma migration at Piton De La Fournaise Volcano from pre-eruptive seismicity. *Geophysical Research Letters*, 46(1), 119–127. <https://doi.org/10.1029/2018GL080895>
- Foulger, G. R., Julian, B. R., Hill, D. P., Pitt, A. M., Malin, P. E., & Shalev, E. (2004). Non-double-couple microearthquakes at Long Valley caldera, California, provide evidence for hydraulic fracturing. *Journal of Volcanology and Geothermal Research*, 132(1), 45–71. [https://doi.org/10.1016/S0377-0273\(03\)00420-7](https://doi.org/10.1016/S0377-0273(03)00420-7)

- Harrington, R. M., & Brodsky, E. E. (2007). Volcanic hybrid earthquakes that are brittle-failure events. *Geophysical Research Letters*, 34(6), L06308. <https://doi.org/10.1029/2006GL028714>
- Huang, H., & Meng, L. (2018). *Episodic magma transport before the eruption of the 2018 Kilauea volcano* (pp. V43J-V0268). Hawaii. Presented at the AGUUF.
- Jousset, P., Budi-Santoso, A., Jolly, A. D., Boichu, M., SuronoDwiyono, S., Dwiyono, S., et al. (2013). Signs of magma ascent in LP and VLP seismic events and link to degassing: An example from the 2010 explosive eruption at Merapi volcano, Indonesia. *Journal of Volcanology and Geothermal Research*, 261, 171–192. <https://doi.org/10.1016/j.jvolgeores.2013.03.014>
- Ketner, D., & Power, J. (2013). Characterization of seismic events during the 2009 eruption of Redoubt Volcano, Alaska. *Journal of Volcanology and Geothermal Research*, 259, 45–62. <https://doi.org/10.1016/j.jvolgeores.2012.10.007>
- Klein, F. W., Koyanagi, R. Y., Nakata, J. S., & Tanigawa, W. R. (1987). The seismicity of Kilauea's magma system In R. W. Decker, T. L. Wright, and P. H. Stauffer (Eds.), *Volcanism in Hawaii, U.S. Geol. Surv. Prof. Pap.*, 1350(2), (chap. 43), pp. 1019–1185. U. S. Geological Survey.
- Lahr, J. C., Chouet, B. A., Stephens, C. D., Power, J. A., & Page, R. A. (1994). Earthquake classification, location, and error analysis in a volcanic environment: Implications for the magmatic system of the 1989–1990 eruptions at redoubt volcano, Alaska. *Journal of Volcanology and Geothermal Research*, 62(1), 137–151. [https://doi.org/10.1016/0377-0273\(94\)90031-0](https://doi.org/10.1016/0377-0273(94)90031-0)
- Matoza, R. S., Shearer, P. M., & Okubo, P. G. (2014). High-precision relocation of long-period events beneath the summit region of Kilauea Volcano, Hawai'i, from 1986 to 2009. *Geophysical Research Letters*, 41(10), 3413–3421. <https://doi.org/10.1002/2014GL059819>
- McNutt, S. R. (1996). Seismic monitoring and eruption forecasting of volcanoes: A review of the state-of-the-art and case histories. In R. Scarpa, & R. I. Tilling (Eds.), *Monitoring and mitigation of volcano hazards* (pp. 99–146): Springer. [https://doi.org/10.1007/978-3-642-80087-0\\_3](https://doi.org/10.1007/978-3-642-80087-0_3)
- McNutt, S. R., & Roman, D. C. (2015). Chapter 59 – volcanic seismicity. In H. Sigurdsson (Ed.), *The encyclopedia of volcanoes* (2nd ed., pp. 1011–1034). Academic Press. <https://doi.org/10.1016/B978-0-12-385938-9.00059-6>
- Neal, C. A., Brantley, S. R., Antolik, L., Babb, J. L., Burgess, M., Calles, K., et al. (2019). The 2018 rift eruption and summit collapse of Kilauea Volcano. *Science*, 363(6425), 367–374. <https://doi.org/10.1126/science.aav7046>
- Neuberg, J., Luckett, R., Baptie, B., & Olsen, K. (2000). Models of tremor and low-frequency earthquake swarms on Montserrat. *Journal of Volcanology and Geothermal Research*, 101(1), 83–104. [https://doi.org/10.1016/S0377-0273\(00\)00169-4](https://doi.org/10.1016/S0377-0273(00)00169-4)
- Neuberg, J. W., Tuffen, H., Collier, L., Green, D., Powell, T., & Dingwell, D. (2006). The trigger mechanism of low-frequency earthquakes on Montserrat. *Journal of Volcanology and Geothermal Research*, 153(1–2), 37–50. <https://doi.org/10.1016/j.jvolgeores.2005.08.008>
- Okubo, P., & Nakata, J. S. (2003). Tectonic pulses during Kilauea's current long-term eruption. In C. Heliker, D. A. Swanson, and T. J. Takahashi (Eds.), *The Pu'u O'o-Kupaianaha eruption of Kilauea volcano, Hawai'i: The first 20 Years, U.S. Geol. Surv. Prof. Pap.*, 1676, (chap. 11, pp. 173–186). U. S. Geological Survey.
- Patrick, M. R., Houghton, B. F., Anderson, K. R., Poland, M. P., Montgomery-Brown, E., Johanson, I., et al. (2020). The cascading origin of the 2018 Kilauea eruption and implications for future forecasting. *Nature Communications*, 11(1), 5646. <https://doi.org/10.1038/s41467-020-19190-1>
- Ross, Z. E., Meier, M., Hauksson, E., & Heaton, T. H. (2018). Generalized seismic phase detection with deep learning. *Bulletin of the Seismological Society of America*, 108(5A), 2894–2901. <https://doi.org/10.1785/0120180080>
- Senobar, N. S., Funning, G. J., Keogh, E., Zhu, Y., Yeh, C. M., Zimmerman, Z., & Mueen, A. (2019). Super-efficient cross-correlation (SEC-C): A fast matched filtering code suitable for desktop computers. *Seismological Research Letters*, 90(1), 322–334. <https://doi.org/10.1785/0220180122>
- Shearer, P. M., Prieto, G. A., & Hauksson, E. (2006). Comprehensive analysis of earthquake source spectra in southern California: Southern California source spectra. *Journal of Geophysical Research*, 111(B6). <https://doi.org/10.1029/2005jb003979>
- Sparks, R. S. J. (2003). Forecasting volcanic eruptions. *Earth and Planetary Science Letters*, 210(1–2), 1–15. [https://doi.org/10.1016/S0012-821X\(03\)00124-9](https://doi.org/10.1016/S0012-821X(03)00124-9)
- Waldhauser, F., & Ellsworth, W. L. (2000). A double-difference Earthquake Location Algorithm: Method and application to the Northern Hayward Fault, California. *Bulletin of the Seismological Society of America*, 90(6), 1353–1368. <https://doi.org/10.1785/0120000006>
- Wech, A. G., & Thelen, W. A. (2015). Linking magma transport structures at Kilauea volcano. *Geophysical Research Letters*, 42(17), 7090–7097. <https://doi.org/10.1002/2015GL064869>
- Withers, M., Aster, R., Young, C., Beiriger, J., Harris, M., Moore, S., & Trujillo, J. (1998). A comparison of select trigger algorithms for automated global seismic phase and event detection. *Bulletin of the Seismological Society of America*, 88(1), 95–106. <https://doi.org/10.1785/bssa0880010095>
- Wolfe, C. J., Okubo, P. G., Ekström, G., Nettles, M., & Shearer, P. M. (2004). Characteristics of deep ( $\geq 13$  km) Hawaiian earthquakes and Hawaiian earthquakes west of  $155.55^{\circ}\text{W}$ . *Geochemistry, Geophysics, Geosystems*, 5(4). <https://doi.org/10.1029/2003GC000618>
- Woods, J., Donaldson, C., White, R. S., Caudron, C., Brandsdóttir, B., Hudson, T. S., & Ágústsdóttir, T. (2018). Long-period seismicity reveals magma pathways above a laterally propagating dyke during the 2014–15 Bárðarbunga rifting event, Iceland. *Earth and Planetary Science Letters*, 490, 216–229. <https://doi.org/10.1016/j.epsl.2018.03.020>
- Yoon, C. E., O'Reilly, O., Bergen, K. J., & Beroza, G. C. (2015). Earthquake detection through computationally efficient similarity search. *Science Advances*, 1(11), e1501057. <https://doi.org/10.1126/sciadv.1501057>
- Zhu, W., & Beroza, G. C. (2018). PhaseNet: A deep-neural-network-based seismic arrival time picking method. *Geophysical Journal International*, 216(1):261–73. <https://doi.org/10.1093/gji/ggy423>